NIH Public Access
Author Manuscript
Acad Radiol. Author manuscript; available in PMC 2013 January 24.

Published in final edited form as:
Acad Radiol. 2012 March ; 19(3): 358–365. doi:10.1016/j.acra.2011.11.010.

CTA Combined with CT Perfusion for Assessing the Efficacy of Anti-angiogenic Therapy in Rabbit VX2 Tumors

Han Wang, MD, PhD, **Lin-Feng Zheng, MD, PhD**, **Yan Feng, MD**, **Xue-Qian Xie, MD**, **Xiao-Ming Yang, MD, PhD**, and **Gui-Xiang Zhang, MD, PhD**
Department of Radiology, Shanghai First People's Hospital, School of Medicine, Shanghai Jiao Tong University, Shanghai 200080, China (H.W., L.-F.Z., Y.F., X.-Q.X., G.-X.Z.); and the Image-Guided Bio-Molecular Interventions Section, Department of Radiology, Institute for Stem Cell and Regenerative Medicine, University of Washington School of Medicine, Seattle, WA 98109 (H.W., X.-M.Y.)

Abstract

Rationale and Objectives—The aim of this study was to validate the feasibility of assessing the efficacy of antiangiogenic therapy on VX2 tumors using three-dimensional computed tomographic (CT) angiography (CTA) combined with CT perfusion.

Materials and Methods—Forty rabbits with VX2 tumors were randomly assigned to four groups according to different doses of antiangiogenic drug, which were administered intraperitoneally daily for 14 days. In each group, 10 animals were scanned using three-dimensional CTA and CT perfusion on days 1 and 2 after the latest administration of the drug. Tumor masses were sectioned, stained by immunohistochemistry, and processed for correlation between CT imaging and histology.

Results—The numbers of new tumor vessels from CTA were significantly different among the four groups ($P < .001$). As the dose of the drug increased, blood flow and blood volume on CT perfusion increased linearly, but the mean transit time and permeability surface-area product decreased linearly ($P < .001$). Immunohistochemical analyses showed that microvascular density decreased, while both luminal vascular number and mature vessel number increased linearly as the drug dose increased ($P < .001$). CT manifestations were correlated well with histologic findings ($P < .05$).

Conclusions—It is feasible to assess the efficacy of antiangiogenic therapy on VX2 tumors using three-dimensional CTA combined with CT perfusion. Three-dimensional CTA can display the morphologic changes of tumor vessels, while CT perfusion can predict the functional changes of tumor vessels after antiangiogenic therapy.

Keywords

Tumor; angiogenesis; CT; angiography; perfusion

Neovascularization is an essential process for the growth, invasion, and metastasis of solid tumors (1,2). Anti-angiogenic therapy represents a promising strategy for tumor therapy. Our understanding of the molecular mechanisms that underlie angiogenesis has advanced significantly over the past decade, leading to the development of a number of new drugs that inhibit angiogenesis (3–5).

© AUR, 2012

Address correspondence to: G.-X.Z. guixiangzhang@sina.com; and X.-M.Y. xmyang@u.washington.edu.

$watermark-text
$watermark-text
$watermark-text

$watermark-text

$watermark-text

$watermark-text

These forms of antiangiogenic therapies have created a need for efficient, noninvasive, and reliable ways to monitor tumor angiogenesis and to assess the efficacy of antiangiogenic therapy. Microvascular density (MVD), particularly measured in the most neovascular area (the “hot spot”) of a tumor, is currently an ideal histologic method in assessing the efficacy of antiangiogenic therapy (6). However, the measurement of MVD is not pragmatic in clinical practice, because of its invasiveness and the inconvenience of obtaining tumor tissues with repeated tumor biopsies.

Molecular imaging and functional imaging represent advances in new imaging technologies (7,8). Recently, tumor angiogenesis has been studied in the laboratories using either fluorescent microscope imaging (9) or microcomputed tomographic (CT) scanning (10). However, these methods were designed for laboratory research with small animals only and cannot be directly applied in a clinical setting on humans. Several medical imaging techniques, including CT imaging, magnetic resonance imaging, and ultrasound, are promising candidates for studying in vivo tumor biology. The increasing clinical use of volume CT imaging and high-field magnetic resonance imaging has made these imaging modalities useful in the investigation of tumor angiogenesis in vivo.

Rabbit models with VX2 tumors have been widely used in preclinical research on either the development of new anti-tumor techniques or the evaluation of tumor response to new antitumor treatment (11–13). The results of our previous work confirmed that it is feasible to monitor dynamic changes in tumor angiogenesis of rabbit VX2 tumors using CT angiography (CTA) with a clinical CT scanner (13). The purpose of the present study was to further validate the feasibility of using CTA combined with CT perfusion to assess the efficacy of antiangiogenic therapy.

MATERIALS AND METHODS

Animal and Tumor Models

Forty New Zealand white rabbits (weight range, 2.0–2.2 kg) were obtained from the Shanghai Experimental Animal Center of the Chinese Academy of Sciences and housed in the animal care facility of the Experimental Animal Center of our institute. The animals were treated in accordance with a protocol that was approved by our institutional animal care and use committee. Each animal was intramuscularly injected with approximately 1×10^7 VX2 tumor cells in the right hind leg and then returned to its cage and fed with standard rabbit food and water ad libitum. The tumor inoculations in all animals were performed by a single investigator (H.W.).

Antiangiogenic Therapy

Starting on the second day after tumor implantation, an anti-angiogenic drug, Endostar (endostatin; Shandong Simcere-Medgenn Bio-Pharmaceutical Corporation, Ltd, Yantai, China), was administered intraperitoneally daily for 14 days. Forty rabbits were randomly divided into four groups of 10 rabbits each. Each rabbit group received a different dose of the antiangiogenic drug as follows. In group A (the negative control group), rabbits were treated with 1 mL saline; in group B, rabbits were treated with 0.15 mg/kg of Endostar; in group C, rabbits were treated with 0.30 mg/kg of Endostar; and in group D, the rabbits were treated with 0.60 mg/kg of Endostar. These treatments in all 40 rabbits were performed by a single investigator (H.W.).

CT Imaging Studies

CT imaging was performed using a 64-row, multidetector CT system (LightSpeed VCT; GE Medical Systems, Milwaukee, WI). Each of the 40 rabbits underwent CTA and CT

$watermark-text

$watermark-text

$watermark-text

perfusion studies. CTA and CT perfusion were carried out on days 1 and 2 after the latest administration of the drug or saline. The rabbits were anesthetized with ketamine (50 mg/kg) and xylazine (Rompun, Selleck Chemicals LLC, Houston, TX) (5 mg/kg) intramuscularly, and a 21-gauge winged infusion set (Surflo, Terumo Europe NV, Leuven, Belgium) was placed in an ear vein for the injection of contrast medium. The infusion sets were placed by a single investigator (H.W.).

CTA—For enhanced CTA scanning, rabbits were placed in the center of the CT scanner and first underwent unenhanced scout scanning from the hip joint to the knee joint. Preliminary experiments confirmed that the early arterial phase, arterial phase, and tumor tissue phase of rabbits began 10, 18, and 36 seconds, respectively, after the injection of contrast medium (13). Accordingly, enhanced CTA was started 10, 18, and 36 seconds after a bolus of iodinated contrast medium (Ultravist 370, 3 mL/kg; Bayer Schering Pharma AG China, Guangzhou, China) was injected into the ear vein. Following the bolus, the injection was continued for 10 seconds at a flow rate of 0.8 mL/s, using an automatic injection system (Stellant Dual, Medrad, Inc, Pittsburgh, PA). All images were acquired using a tube voltage of 180 kVp, a tube current of 30 mA, a slice thickness of 0.625 mm, a field of view of 180 mm, 160 slices, and the standard algorithm. The CT angiographic scans in all 40 animals were performed by a single investigator (H.W.).

CT perfusion—Rabbits were placed in the center of the CT scanner and first underwent unenhanced scout scanning through the tumors to enable the selection of the appropriate transverse level for perfusion scanning. Then, perfusion scanning was started 1 second before a bolus injection of iodinated contrast medium (Ultravist 370, 3 mL/kg) via the ear vein. Following the bolus, the injection was continued for 10 seconds at a flow rate of 0.8 mL/s, using an automatic injection system (Stellant Dual). Scanning was continued for 45 seconds at a speed of 1.5 seconds per rotation. All images were acquired using a tube voltage of 120 kVp, a tube current of 100 mA, a slice thickness of 2.5 mm, a field of view of 180 mm, and 16 slices. The CT perfusion scans in all 40 animals were performed by a single investigator (H.W.).

Histopathology and Immunohistochemistry

Histopathology—Each of the rabbits was anesthetized using ketamine (50 mg/kg) and xylazine (5 mg/kg) intramuscularly, and the thoracic cavity and pericardium were opened. A 5-Fr catheter was inserted through the left ventricular wall into the ascending aorta. A small outlet window of the wall of the right auricle was created to allow the egress of blood and perfusate. Each animal was perfused with 4,500 mL 10% formalin in saline containing 12,500 IU heparin. After perfusion, the muscle and soft tissue that encapsulated each VX2 tumor were bluntly dissected, and the tumor was resected, and then embedded for sectioning at 5-μm thickness. For each of the four groups, the histologic slides corresponded to the parallel CT perfusion sections obtained in each tumor. Briefly, we embedded the resected tumors in 10% paraffin for 48 hours according to the position of the CT scan. Then, the sizes of tumor masses were measured from the starting scan to the ending scan. Subsequently, according to the numbers of slides on CT imaging, we selected the histologic slides at equal intervals, so that the histologic slides matched the CT imaging slices. Finally, the histologic slides were stained using the endothelium-specific CD31 antibody as described below.

Immunohistochemistry—Immunohistochemistry was performed using previously reported method (11). Briefly, histologic slides were first incubated with 3% hydrogen peroxide in methanol for 10 minutes. After blocking nonspecific protein-binding sites with 5% bovine serum albumin (Sigma Chemical, St Louis, MO) for 1 hour, the slides were incubated with a 1:500 dilution of mouse monoclonal antirabbit CD31 antibody (Lab

Vision/NeoMarkers, Fremont, CA) at 4°C overnight. Control slices were incubated with phosphate-buffered saline only. Then, slices were incubated with peroxidase-conjugated goat antimouse secondary antibody at 1:200 dilution (Serotec, Indianapolis, IN). The slides were subsequently stained with diaminobenzidine (Stable DAB; Research Genetics, Huntsville, AL) and then counterstained with hematoxylin (Sigma-Aldrich, St Louis, MO).

Image Analysis

CT angiographic data were reconstructed using volume rendering and maximum intensity projection, while CT perfusion data were reconstructed using perfusion maps. All images were reconstructed onto a 512 × 512 pixel matrix using Advantage Workstation 4.4 (GE Medical Systems, Milwaukee, WI).

All images were interpreted on a 2,000 × 2,000 picture archiving and communication system monitor (PathSpeed; GE Medical Systems Integrated Imaging Solutions, Mt Prospect, IL) with appropriate adjustment of the optimal window settings. Analyses represented the consensus between two experienced radiologists. In this process, the two radiologists were blinded to every subject's dose assignment until the completion of image analysis.

The numbers of new vessel branches within each tumor in the different groups were determined on CT angiographic images. The morphology of tumor vessels within the different groups was recorded. Maximum intensity projection images of the phase and reconstruction plane that displayed vessels most clearly were chosen for counting the numbers of new vessel branches. The absolute values of four perfusion parameters (blood flow [BF], blood volume [BV], mean transit time [MTT], and permeability surface-area product [PS]) were measured and calculated on the basis of regions of interest on all slices of the tumors.

Histopathologic and Immunohistochemical Analyses

For tumors in each rabbit group, MVD and luminal vascular number (LVN) were recorded on CD31-stained slides. For the purpose of counting MVD, any CD31-highlighted endothelial cell or cell cluster that was clearly separate from adjacent tissue elements was counted as a single countable microvessel (6). Briefly, the entire tumor slides were observed microscopically at original magnifications of 100×, and the area with the largest number of microvessels (the hot spot) was identified. Then, the MVD and LVN were counted in that hot-spot area with the use of original magnification 200×. For LVN, only the CD31-highlighted endothelial cell cluster that formed a discernible microvessel lumen was counted (14). During counting, the LVN was further divided into two categories (Fig 1): (1) mature tumor vessels (those with a complete endothelial cell wall and layers of smooth muscle cells; Fig 1a), and (2) immature tumor vessels (those with an incomplete layer of endothelial cell wall; Fig 1b). All aforementioned immunohistochemical parameters were counted three times in the different hot-spot areas, and then the mean values of MVD, LVN, mature vessel number (MVN), immature vessel number (IVN), and the percentage of MVN in LVN were recorded, respectively. The microstructure of mature or immature tumor vessels was observed microscopically at original magnification of 400×.

Statistical Analysis

All data are presented as mean ± standard deviation. Analysis of variance was carried out on the numbers of new-vessel branches in each tumor; the values of four perfusion parameters (BF, BV, MTT, and PS); and the MVD, LVN, MVN, IVN, and the percentage of MVN in LVN of tumors in all four groups. If the results of analysis of variance were significantly different between groups, analysis of the least significant difference was carried out with a comparison of the aforesaid parameters in each group. Pearson's correlation coefficient (r)

$watermark-text $watermark-text $watermark-text

$watermark-text

$watermark-text

$watermark-text

was used to investigate the relationships among imaging manifestations and histologic findings, as well as the dose levels of drug. All statistical results were calculated using SAS version 8.0 (SAS Institute Inc, Cary, NC). P values < .05 were considered to indicate a statistically significant difference.

RESULTS

Numbers of New Tumor Vessel Branches on CTA

Table 1 shows the numbers of new tumor vessel branches shown on CT angiographic maximum intensity projection images for each animal group. The numbers of new vessel branches in tumors from each group measured using CTA were significantly different ($P < .001$). The numbers of new vessels reduced linearly from group A to group D (all $P < .001$).

Morphologic Features of Tumor Vessels after Antiangiogenic Therapy on CTA

Figures 2 and 3 show the morphologic features of tumor vessels of each animal group demonstrated by the CT angiographic images. The tumor vessels of the negative control group (Figs 2a and 3a) showed the dilated preexisting feeder artery and immature tumor vessel webs containing numerous tortuous, dilated, irregular vessels that penetrated the tumor. After antiangiogenic therapy, as the dose of drug administrated increased, the sizes of the preexisting feeder arteries became smaller, and the numbers of new vessels reduced. In addition, the new vessels were displayed clearly and the morphologic features returned to straight and regular in the groups that received increasing doses of drug (Figs 2b–d and 3b–d).

Efficacy of Antiangiogenic Therapy with Different Doses of Endostatin on CT Perfusion Maps

Figure 4 shows the CT perfusion maps of tumors in each animal group. Table 2 shows the absolute values of four perfusion parameters (BF, BV, MTT, and PS), calculated on CT perfusion maps for each group. The values of BF, BV, MTT, and PS were significantly different among the four animal groups ($P < .001$), demonstrating that the values of BF and BV increased linearly from group A to group D (all P values < .001). However, the values of MTT and PS decreased linearly from group A to group D (all P values < .001). Significant positive correlations were observed between the dose level of endostatin and the values of BF and BV ($r = 0.936$ and $r = 0.901$, respectively, $P < .001$ for both), whereas significant negative correlations were observed between the drug's dose level and the values of MTT and PS ($r = -0.886$ and $r = -0.629$, respectively, $P < .001$ for both).

Immunohistochemistry

CD31 immunohistochemistry of the tumor tissues of each group is demonstrated in Figure 5 and Table 3. The results revealed that the MVD values were significantly lower after antiangiogenic therapy ($P < .001$). As the dose of endostatin increased, the MVD values progressively decreased, and the difference between the values in each group was significant (all P values < .001). Both the LVN values and the MVN values increased significantly (all P values < .001) as the dose of endostatin increased. The percentage of MVN in LVN significantly higher in all three antiangiogenic groups than in the control group (all P values < .05), while no significant difference of this parameter was observed between the antiangiogenic groups.

CT Imaging and Histologic Correlations

Correlations between CT imaging results and histologic findings are presented in Table 4. Significant positive correlations were observed between the values of BF and BV and the

values of LVN and MVN (all *P* values < .001), as well as between the values of MTT and PS and the value of MVD (*P* < .001). Significant negative correlations were observed between the values of MTT and PS and the values of LVN and MVN (all *P* values < .001), as well as between the values of BF and BV and the value of MVD (*P* < .001).

DISCUSSION

In this study, we investigated the role of CTA and CT perfusion in assessing the efficacy of tumor antiangiogenic therapy by examining the changes in CT angiographic imaging and perfusion parameters after antiangiogenic therapy with endostatin in a rabbit VX2 tumor model.

One of the advances in clinical CT imaging in the past decade is the multidetector technology available, including scanners with 4, 8, 16, 64, 256, and 320 rows. This increasing capacity of multidetector technology has greatly enhanced the ability using computed tomography to image those organs with more small-sized arteries, such as the renal, coronary, and intracranial arteries (15–17). This imaging modality shows high efficacy not only in terms of spatial resolution but also in temporal resolution. In addition, the improving resolution of clinical CT scanning has enabled using this imaging modality to study tumor angiogenesis and antiangiogenic therapy in vivo.

As the results of our previous work (13) demonstrated, it is feasible to monitor tumor angiogenesis dynamically using CTA with a clinical CT scanner in rabbit models with VX2 tumors. In the present study, we specifically investigated the efficacy of using CTA combined with CT perfusion scanning to assess antiangiogenic therapy efficacy in the same tumor models using clinical 64-row multidetector CT imaging.

Endostatin, which was discovered in 1997 (18), has been the most intensively studied human endogenous angiogenesis inhibitor. It is a fragment of collagen XVIII, and it stimulates apoptosis in proliferating endothelial cells of pathologically growing vessels. It also possesses other antiangiogenic actions. For example, several previous studies have confirmed that recombinant endostatin can effectively inhibit angiogenesis and the growth of various solid tumors as well as their metastases (19), without considerable side effects, drug toxicity, or drug resistance (20). Therefore, this protein is a promising antitumor drug (21). In the present study, we chose Endostar as the antiangiogenic agent. More recently, Endostar was confirmed to be also effective in other kinds of solid cancer, including gastric cancer (22) and breast cancer (23). However, the change of vessel and blood-flow within the tumor after its action has been unknown.

Studies on physiologic angiogenesis resulted in the discovery of a phenomenon known as “vascular pruning.” The essence of this phenomenon is the strict regulation of angiogenesis by the balance of proangiogenic and antiangiogenic factors depending on the stage of development of the organism (24). In tumor antiangiogenic therapy by endostatin or other antiangiogenic factors, vascular pruning occurs. The potential mechanisms for this phenomenon include that (1) endotheliocytes from preexisting vessels are resistant to apoptotic stimuli, in a similar manner to cells of postangiogenic vessels with mature endotheliocytes (25), and (2) any slight disorder in the process of coordinated angiogenesis can induce apoptosis of endotheliocytes and the degradation of an unformed vessel (26,27). Therefore, some authors have introduced a new concept of the normalization of tumor vasculature in antiangiogenic therapy (25,26). According to this hypothesis, antiangiogenic drugs, such as endostatin, result in the apoptosis of unformed intratumor microvessels and the maturing of preexisting intratumor microvessels (25). This normalization of vasculature within tumor increases the delivery of oxygen and therapeutics and thereby enhances the

$watermark-text $watermark-text $watermark-text

$watermark-text

$watermark-text

$watermark-text

efficacy of radiotherapy on the tumor (28,29). Most recently, a research team reported that there are both morphologic and functional changes after vascular endothelial growth factor–targeted antiangiogenic therapy on glioma blood vessels using in vivo multiphoton laser scanning microscopy and confirmed that antiangiogenic therapy has a dose-dependent effect both on morphologic and functional changes of tumor vessels (30).

In the present study, CTA demonstrated a significant dose-dependent reduction in the numbers of new tumor vessel branches in tumors after treatment with Endostar (Table 1). In addition, we found that the morphologic features of the tumor vessels also changed after treatment with Endostar. After antiangiogenic therapy, as the dose of Endostar increased, the sizes of the preexisting feeder arteries became smaller, and the numbers of new vessels also decreased. In addition, new vessels were clearly displayed, and their morphologic features returned to normal with increasing doses of Endostar (Figs 2b–d and 3b–d). These findings not only confirm previous reports of the phenomenon of “vascular pruning” or “normalization” actions for tumor vessels after antiangiogenic treatment but also indicate that this action is relative to the dose of endostatin within a certain dose window.

CT perfusion is an advanced imaging technique that can provide pathophysiologic information by quantifying tissue hemodynamics (14,31,32). This technique acquires dynamic time-attenuation data by a consecutive multislice scan at a fixed tissue section after an intravenous bolus injection of contrast medium. These time-attenuation data directly reflect the dynamic change in the density of target tissue and indirectly reflect the change of blood perfusion of target tissue after contrast medium injection. The perfusion maps are generated by image reconstruction on a pixel-by-pixel basis and artificial color map processing of the perfusion parameters. In this way, the perfusion status of the target tissue is evaluated quantitatively. There are four parameters of CT perfusion: (1) the BF value, which reflects the assemblage rate per unit of target tissue to BF in the first scan after contrast injection; (2) the BV value, which reflects the total blood vessel volume of the target tissue; (3) the MTT value, which indicates the mean time for the contrast medium to flow through blood vessels; and (4) the PS value, which reflects a one-way transmission speed for contrast medium diffusion into cell spaces via the vascular endothelial interspaces.

In the present study, the values of BF and BV of the tumors in the groups treated with Endostar were significant higher than those of the tumors in the negative control group. In addition, we found that the values of BF and BV increased linearly in the tumors of groups B, C, and D, which significantly correlated with the increasing dose of the drug. However, the values of MTT and PS of the tumors in the anti-angiogenic drug–treated groups were significantly lower than those of the tumors in the negative control group. The values of MTT and PS showed linear reductions in tumors in groups B, C, and D, which also significantly correlated with the dose of the drug. In correlation to histology, we also observed in the CD31-stained tumor tissue sections that as the dose of the antiangiogenic drug increased, the MVD value decreased, while the values of LVN and MVN both increased. The results of correlation studies confirm that there are significant positive correlations between the values of BF and BV and the values of LVN and MVN, as well as between the values of MTT and PS and the value of MVD. In addition, there are significant negative correlations between the values of MTT and PS and the values of LVN and MVN as well as between the values of BF and BV and the value of MVD. We consider that the increase in the values of BF and the decrease in the value of MTT after treatment with the antiangiogenic drug are due to the luminal vessels, including mature vessels, which make the blood or contrast medium flow through the tumor tissue more easily. The value of BV increased after drug-treated is because the luminal vessels make the tankage of blood in tumor tissue increase. The reduction in the PS value after the antiangiogenic treatment resulted from the reduction in MVD, which decreased the vascular endothelial interspace.

These findings are consistent with CT perfusion studies on antiangiogenic therapy from other groups (14,30). These studies demonstrated a decrease in vascular permeability and an increase in BF velocity of tumor vessel after therapy.

CONCLUSIONS

The results of this study suggest that it is feasible to use CTA combined with CT perfusion to assess the efficacy of antiangiogenic therapy on tumors. CTA enables display of the morphologic changes of tumor vessels, while CT perfusion can predict functional changes of tumor vessels after antiangiogenic therapy.

Acknowledgments

Dr Wang thanks the Morning Star Youth Scholar Project of Shanghai Jiao Tong University (2010) and the Top 100 Youth Scholar Project of Shanghai Jiao Tong University School of Medicine (2011) for support.

This work was supported by grant 30901730 from the National Natural Science Foundation of China, grant 20090073110072 from the Fund of Ministry of Education of China, grant 1052nm05800 from the Fund of the Science and Technology Commission of Shanghai Municipality, and grant 2008Y108 from the Fund of Youth Research Program of Health Administration Bureau of Shanghai Municipality.

References

1. Folkman J. Fundamental concepts of the angiogenic process. Curr Mol Med. 2003; 3:643–651. [PubMed: 14601638]
2. Folkman J. Is angiogenesis an organizing principle in biology and medicine? J Pediatr Surg. 2007; 42:1–11. [PubMed: 17208533]
3. Ellis LM, Hicklin DJ. VEGF-targeted therapy: mechanisms of anti-tumour activity. Nat Rev Cancer. 2008; 8:579–591. [PubMed: 18596824]
4. Folkman J. Antiangiogenesis in cancer therapy—endostatin and its mechanisms of action. Exp Cell Res. 2006; 312:594–607. [PubMed: 16376330]
5. Gaya AM, Rustin GJ. Vascular disrupting agents: a new class of drug in cancer therapy. Clin Oncol. 2005; 17:277–290.
6. Nieto Y, Woods J, Jones RB, et al. Prognostic analysis of intratumor microvessel density (MVD) and vascular endothelial growth factor (VEGF) in high-risk primary breast cancer (HRPBC) patients (PTS) receiving high-dose chemotherapy (HDC). J Clin Oncol. 2005; 23:27s–s.
7. Cai WB, Chen XY. Multimodality molecular imaging of tumor angiogenesis. J Nucl Med. 2008; 49:113s–128s. [PubMed: 18523069]
8. Folkman J, Beckner K. Angiogenesis imaging. Acad Radiol. 2000; 7:783–785. [PubMed: 11048875]
9. Dunphy MP, Entenberg D, Toledo-Crow R, et al. In vivo microcartography and subcellular imaging of tumor angiogenesis: a novel platform for translational angiogenesis research. Microvas Res. 2009; 78:51–56.
10. Zagorchev L, Mulligan-Kehoe MJ. Molecular imaging of vessels in mouse models of disease. Eur J Radiol. 2009; 70:305–311. [PubMed: 19304428]
11. Wu H, Exner AA, Shi H, et al. Dynamic evolutionary changes in blood flow measured by MDCT in a hepatic VX2 tumor implant over an extended 28-day growth period: time-density curve analysis. Acad Radiol. 2009; 16:1483–1492. [PubMed: 19896066]
12. Qi XL, Liu J, Burns PN, et al. The characteristics of vascular growth in VX2 tumor measured by MRI and micro-CT. J Oncol. 2012; 2012:362096. [PubMed: 21941548]
13. Wang H, Zheng LF, Feng Y, et al. A comparison of 3D-CTA and 4D-CE-MRA for the dynamic monitoring of angiogenesis in a rabbit VX2 tumor. Eur J Radiol. 2012; 81:104–110. [PubMed: 20413238]
14. Kan ZX, Phongkitkarun S, Kobayashi S, et al. Functional CT for quantifying tumor perfusion in antiangiogenic therapy in a rat model. Radiology. 2005; 237:151–158. [PubMed: 16183931]

$watermark-text $watermark-text $watermark-text

$watermark-text
$watermark-text
$watermark-text

15. Halpern EJ, Levin DC, Zhang S, et al. Comparison of image quality and arterial enhancement with a dedicated coronary CTA protocol versus a triple rule-out coronary CTA protocol. Acad Radiol. 2009; 16:1039–1048. [PubMed: 19523852]
16. de Graaf FR, van Velzen JE, Witkowska AJ, et al. Diagnostic performance of 320-slice multidetector computed tomography coronary angiography in patients after coronary artery bypass grafting. Eur Radiol. 2011; 21:2285–2296. [PubMed: 21735068]
17. Sugihara R, Kitajima K, Maeda T, et al. Comparison of capability of abdominal 320-detector row CT and of 16-detector row CT for small vasculature assessment. Kobe J Med Sci. 2011; 56:E154–E161. [PubMed: 21937862]
18. O'Reilly MS, Boehm T, Shing Y, et al. Endostatin: an endogenous inhibitor of angiogenesis and tumor growth. Cell. 1997; 88:277–285. [PubMed: 9008168]
19. Boehm T, Folkman J, Browder T, et al. Antiangiogenic therapy of experimental cancer does not induce acquired drug resistance. Nature. 1997; 390:404–407. [PubMed: 9389480]
20. Digtyar AV, Pozdnyakova NV, Feldman NB, et al. Endostatin: current concepts about its biological role and mechanisms of action. Biochemistry (Mosc). 2007; 72:235–246. [PubMed: 17447877]
21. Sun L, Ye HY, Zhang YH, et al. Epidermal growth factor receptor antibody plus recombinant human endostatin in treatment of hepatic metastases after remnant gastric cancer resection. World J Gastroenterol. 2007; 13:6115–6118. [PubMed: 18023113]
22. Lu N, Ling Y, Gao Y, et al. Endostar suppresses invasion through downregulating the expression of matrix metalloproteinase-2/9 in MDA-MB-435 human breast cancer cells. Exp Biol Med (Maywood). 2008; 233:1013–1020. [PubMed: 18480415]
23. Stupack DG, Cheresh DA. Apoptotic cues from the extracellular matrix: regulators of angiogenesis. Oncogene. 2003; 22:9022–9029. [PubMed: 14663480]
24. Witte L, Hicklin DJ, Zhu ZP, et al. Monoclonal antibodies targeting the VEGF receptor-2 (Flk1/KDR) as an anti-angiogenic therapeutic strategy. Cancer Metastasis Rev. 1998; 17:155–161. [PubMed: 9770111]
25. Jain RK. Normalization of tumor vasculature: an emerging concept in anti-angiogenic therapy. Science. 2005; 307:58–62. [PubMed: 15637262]
26. Tong RT, Boucher Y, Kozin SV, et al. Vascular normalization by vascular endothelial growth factor receptor 2 blockade induces a pressure gradient across the vasculature and improves drug penetration in tumors. Cancer Res. 2004; 64:3731–3736. [PubMed: 15172975]
27. Winkler F, Kozin SV, Tong RT, et al. Kinetics of vascular normalization by VEGFR2 blockade governs brain tumor response to radiation: role of oxygenation, angiopoietin-1, and matrix metalloproteinases. Cancer Cell. 2004; 6:553–563. [PubMed: 15607960]
28. Matsumoto S, Batra S, Saito K, et al. Anti-angiogenic agent sunitinib transiently increases tumor oxygenation and suppresses cycling hypoxia. Cancer Res. 2011; 71:6350–6359. [PubMed: 21878530]
29. Goel S, Duda DG, Xu L, et al. Normalization of the vasculature for treatment of cancer and other diseases. Physiol Rev. 2011; 91:1071–1121. [PubMed: 21742796]
30. von Baumgarten L, Brucker D, Tirniceru A, et al. Bevacizumab has differential and dose-dependent effects on glioma blood vessels and tumor cells. Clin Cancer Res. 2011; 17:6192–6205. [PubMed: 21788357]
31. Meijerink MR, van Cruijsen H, Hoekman K, et al. The use of perfusion CT for the evaluation of therapy combining AZD2171 with gefitinib in cancer patients. Eur Radiol. 2007; 17:1700–1713. [PubMed: 17072618]
32. Ng CS, Chandler AG, Wei W, et al. Reproducibility of CT perfusion parameters in liver tumors and normal liver. Radiology. 2011; 260:762–770. [PubMed: 21788525]

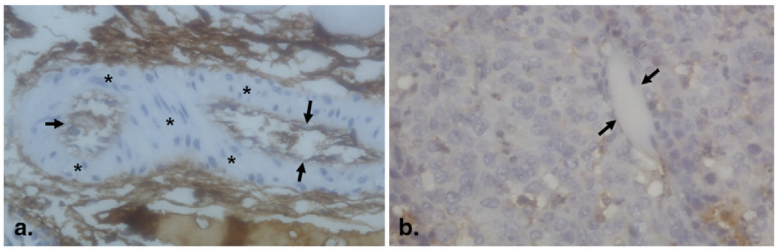

Figure 1.

Microscope images show the two categories of luminal vessel in tumor: **(a)** mature vessel, with a complete endothelial cell wall *(arrow)* and layers of smooth muscle cells *(star)*, and **(b)** immature tumor vessels, with an incomplete layer of endothelial cell wall *(arrow)*. CD31 stain, original magnification 400×.

$watermark-text
$watermark-text
$watermark-text

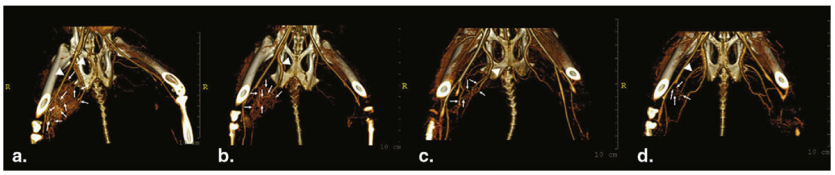

Figure 2.

Reconstructed computed tomographic angiographic images **(a–d)** showing new tumor vessels *(arrows)* as well as preexisting tumor feeder arteries *(arrowheads)* in groups **a** to **d**, respectively. The numbers of new tumor vessels of negative control group (group **a**) are greater than those of antiangiogenic drug–treated groups (groups **b, c**, and **d**). As the dose of administrated drug increased, the numbers of new tumor vessels reduced. Among the three treated groups, the new tumor vessels of group **b** were more prominent than those of groups **c** and **d**.

$watermark-text
$watermark-text
$watermark-text

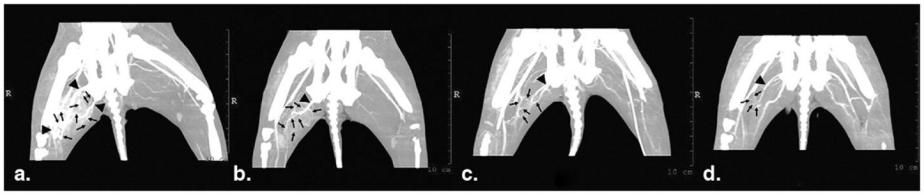

Figure 3.

Reconstructed computed tomographic angiographic maximum intensity projection images **(a–d)** presenting new tumor vessels *(arrows)* as well as preexisting tumor feeder arteries *(arrowheads)* in groups **a** to **d**, respectively. The characteristics of tumor vessels among different groups are similar to those shown in Figure 2.

$watermark-text
$watermark-text
$watermark-text

$watermark-text

$watermark-text

$watermark-text

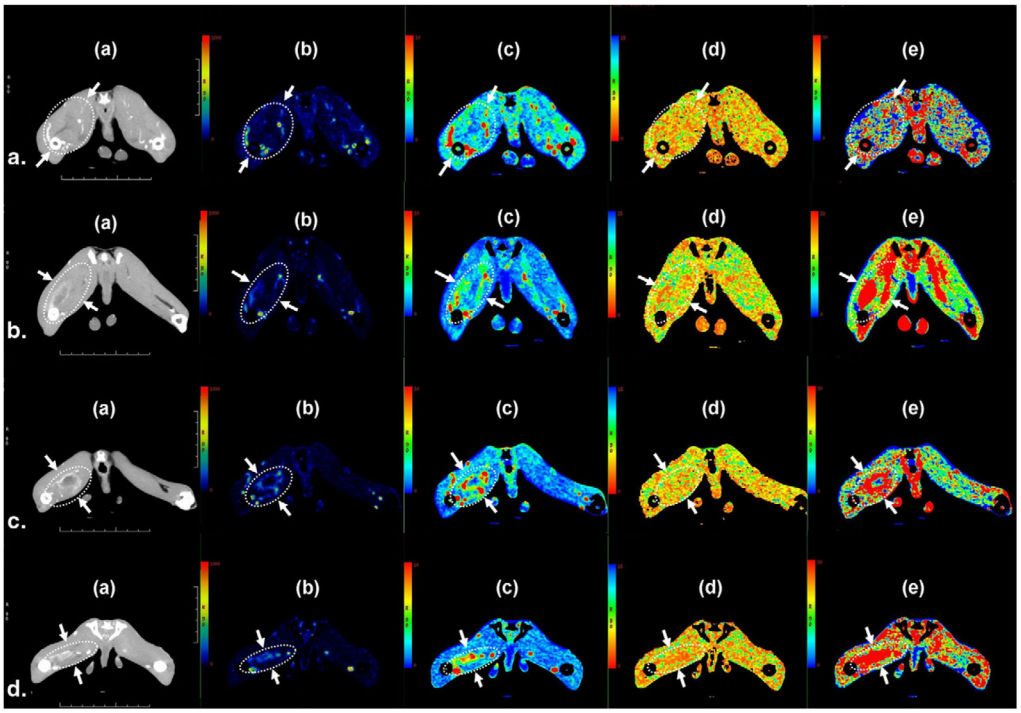

Figure 4.

Computed tomographic (CT) perfusion maps of tumors among the four animal groups. Rows A to D represent groups A to D, respectively. In each row, image **(a)** is the contrast-enhancement CT image of the largest size cross-section of tumor, and images **(b)** to **(e)** are the perfusion map images, including **(b)** blood flow, **(c)** blood volume, **(d)** mean transit time, and **(e)** permeability surface of the same cross-section. The *elliptical dashed lines* and *arrows* highlight the tumor area. The color spectrum indicates the value of the perfusion parameter, ranging from high *(red)* to low *(blue)*.

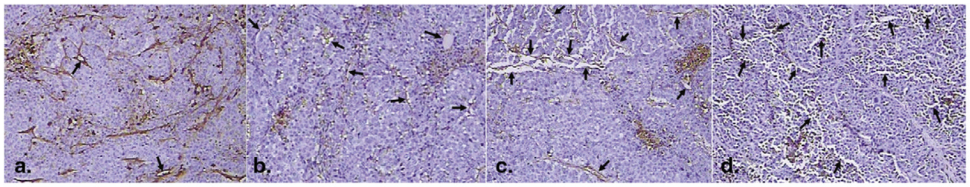

Figure 5.

Immunohistochemical staining of tumor tissue sections for the specific endothelial antigen CD31 **(a–d)** shows the tumor tissues of groups **a** to **d**, respectively. The luminal microvascular structures *(arrows)* in tumors increased as the dose of endostatin increased. Original magnification 100×.

$watermark-text
$watermark-text
$watermark-text

$watermark-text

$watermark-text

$watermark-text

TABLE 1

Numbers of New Vessel Branches in Tumors From Each Group ($n = 10$)

Group	Number of New Tumor Vessel Branches	LSD
A	22.3 ± 2.1	
B	13.9 ± 1.6	$P < .001$
C	10.8 ± 1.2	$P < .001$
D	7.0 ± 1.3	$P < .001$
ANOVA	$P < .001$	

ANOVA, analysis of variance; LSD, least significant difference.

$watermark-text $watermark-text $watermark-text

TABLE 2

Values of BF, BV, MTT, and PS of Tumors, as Calculated on CT Perfusion Maps ($n = 10$)

Group	BF (mL/min/100 g)	BV (mL/100 g)	MTT (seconds)	PS (mL/min/100 g)	LSD
A	38.9 ± 2.7	13.6 ± 1.7	29.8 ± 2.9	56.6 ± 12.1	
B	53.2 ± 5.9	26.9 ± 3.7	25.0 ± 1.6	47.7 ± 11.3	$P < .001$
C	78.5 ± 7.0	33.0 ± 3.3	20.6 ± 1.7	38.9 ± 12.3	$P < .001$
D	95.3 ± 9.7	41.5 ± 5.7	17.5 ± 1.8	31.6 ± 11.5	$P < .001$
Analysis of variance	$P < .001$	$P < .001$	$P < .001$	$P < .001$	

ANOVA, analysis of variance; BF, blood flow; BV, blood volume; CT, computed tomographic; LSD, least significant difference; MTT, mean transit time; PS, permeability surface-area product.

$watermark-text $watermark-text $watermark-text

TABLE 3

MVD, LVN, MVN, IVN, and the Percentage of MVN in LVN of Each Group ($n = 10$)

Group	MVD	LVN	MVN	IVN	MVN in LVN (%)	LSD
A	40.7 ± 3.4	1.3 ± 0.6	0.2 ± 0.1	1.2 ± 0.5	11.1 ± 2.1	
B	30.8 ± 4.1	3.2 ± 0.7	0.5 ± 0.2	2.7 ± 1.2	13.3 ± 1.3	$P < .001$
C	20.2 ± 2.8	6.0 ± 1.4	0.8 ± 0.4	5.7 ± 1.6	14.7 ± 2.7	$P < .001$
D	16.7 ± 1.6	8.7 ± 1.5	1.2 ± 0.5	7.6 ± 1.3	15.0 ± 2.8	$P < .001$
ANOVA	$P < .001$	$P < .001$	$P < .001$	$P < .001$	$P = .002$	

ANOVA, analysis of variance; IVN, immature vessel number; LSD, least significant difference; LVN, luminal vascular number; MVD, microvascular density; MVN, mature vessel number.

$watermark-text

$watermark-text

$watermark-text

TABLE 4

Pearson's Correlations (*P* Values) and Associated Significance Levels Between the CT Perfusion Parameters and Histologic Findings ($n = 10$)

	BF	BV	MTT	PS
MVD	−0.814 (<.001)	−0.861 (<.001)	0.976 (<.001)	0.825 (<.001)
LVN	0.992 (<.001)	0.950 (<.001)	−0.747 (<.001)	−0.362 (.022)
MVN	0.912 (<.001)	0.929 (<.001)	−0.596 (<.001)	−0.194 (.230)

BF, blood flow; BV, blood volume; CT, computed tomographic; LVN, luminal vascular number; MTT, mean transit time; MVD, microvascular density; MVN, mature vessel number; PS, permeability surface-area product.